ABSTRACT

The drag crisis for spheres falling in liquid helium II has been found to occur at a Reynolds number of about 5×10^5 based on currently available values of the kinematic viscosity. From the presence of the drag crisis and on the assumption of suppression of boundary layer turbulence at higher Reynolds numbers, strong evidence for the "ordinary fluid" concept of He II at super-critical velocities is found.

ACKNOWLEDGEMENTS

I wish to express my appreciation to Dr. C.B. Benson for his suggestion of the problem, and for his help and guidance throughout the work.

Also, I would like to thank the technicians of the department, Messrs. Auxier, Goodchild and Hart, who helped me in my work. I am particularly grateful to Mr. J. Rosalmair whose aid in rebuilding the cryostat and the manufacture of spheres was invaluable.

Finally, I am much indebted to Mr. D. Gedke for his help in the design of the electronic system; and to Miss P. Chrysler and the staff of the Computing Centre of the University of Ottawa for facilitating the calculation of the experimental parameters by setting up a computing program.

TABLE OF CONTENTS

LIST OF FIGURES

CHAPTER I

INTRODUCTORY IDEAS

I.I Newton's Resistance Law

A body in steady motion through a fluid at rest experiences a force in a direction opposite to that of the motion. This force is called the "drag" or "resistance".

The first attempt to formulate a hydrodynamic resistance law was made by Newton who considered the case of a body moving through a medium of noninteracting, static point masses. The body impacts with, and thus imparts momentum to the particles... each of which experiences an 'inertia force' (the product of its mass and acceleration).

The force (D) exerted by the fluid on the body equals the rate of change of momentum of the particles in the fluid due to the body. That is:

$$D = (\rho AV)V' \qquad (I)$$

where

ρ - fluid density

A - cross-sectional area of the body perpendicular to its direction of motion

V - body velocity

V' - velocity imparted to the particles.

CHAPTER I

INTRODUCTORY IDEAS

I.I Newton's Resistance Law

A body in steady motion through a fluid at rest experiences a force in a direction opposite to that of the motion. This force is called the "drag" or "resistance".

The first attempt to formulate a hydrodynamic resistance law was made by Newton who considered the case of a body moving through a medium of noninteracting, static point masses. The body impacts with, and thus imparts momentum to the particles... each of which experiences an 'inertia force' (the product of its mass and acceleration).

The force (D) exerted by the fluid on the body equals the rate of change of momentum of the particles in the fluid due to the body. That is:

$$D = (\rho AV)V' \qquad (I)$$

where

ρ - fluid density

A - cross-sectional area of the body perpendicular to its direction of motion

V - body velocity

V' - velocity imparted to the particles.

If V' is proportional to V, then

$$D = f\rho AV^2 \qquad (2)$$

where 'f' is the proportionality constant. Equation (2) is known as Newton's Resistance Law. The experimental values of the proportionality constant of Newton's Resistance Law applied to real fluids do not, in general, agree with theoretical ones. The source of this disagreement lies primarily in the assumption of noninteracting point masses.

In a real fluid particles do interact. Viscous forces as well as inertia forces arise in the displacement of a particle from in front of a body. The viscosity of the fluid has two main effects.

1: A 'boundary layer', in which there is a velocity gradient, is formed on the wall of the body moving through the fluid. The body thus experiences a viscous force.... the "skin friction" or "friction drag".

2: The paths of particles about a body are changed as a result of the formation of a boundary layer and vortices. Thus the pressure distribution at the body surface changes to such an extent that the resultant of the pressure forces is not zero. The body thus experiences a "pressure drag".

Hence, viscous as well as inertia forces require consideration for motions in real fluids.

I.2 The Drag Coefficient, and the Reynolds' Number

In spite of the deficiencies of Newton's Resistance Law, it has become customary to write the drag force (D) in the form

$$D = \frac{C\rho AV^2}{2} \qquad (3)$$

for which C, the "drag coefficient", is experimentally determined for various bodies.

It is found that C is a function of the ratio of inertia forces to viscous forces acting in the system. This ratio is called the Reynolds' number which is defined by the relation

$$R = \frac{VL}{\nu} \qquad (4)$$

where, for a body moving through the fluid,

V - velocity of the body

L — characteristic length of the body

ν - kinematic viscosity of the fluid

The functional relationship between C and R absorbs the variations arising from the viscous (and possibly other) effects. Its knowledge enables us to calculate the drag on a body of given shape for all fluids, velocities, and body dimensions. The relation itself however, must be ascertained by

experiment for each shape and body position. That is: to each shape and body position, there belongs a characteristic function $C = F(R)$.

The characteristic C vs. R curve for spheres (1) is shown in Fig. A. Stokes' theoretical law holds to $R \approx 1$. With increasing Reynolds number, the drag coefficient falls and becomes approximately constant at a value of $C \approx .45$ for $R \approx 2 \times 10^3$ to 2×10^5. At $R \approx 3 \times 10^5$ the sudden decrease in the drag coefficient, called the 'drag crisis', marks the onset of turbulence in the boundary layer.

As will be outlined in the following chapter, the knowledge of this characteristic function provides one means of comparing the hydrodynamical behaviour of helium II with that of ordinary fluids.

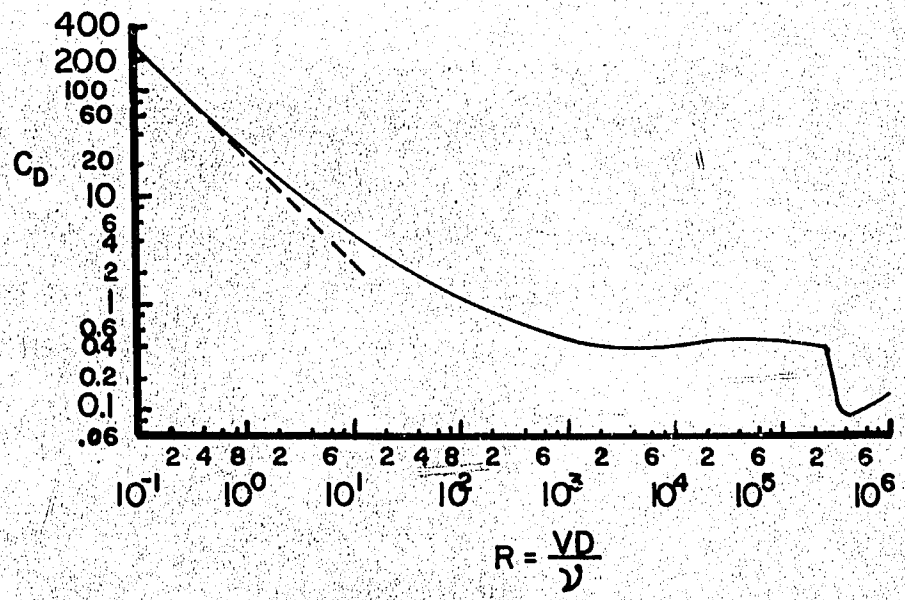

Fig. A Experimental drag coefficients of the sphere as a function of Reynolds number.

CHAPTER 2

MEASUREMENTS OF DRAG IN LIQUID HELIUM II

2.I Theoretical Considerations

The 'superfluid' characteristics of liquid helium II and their explanation through the "two-fluid model" are well known — as are, therefore some of its differences from ordinary fluids (2).

Of primary importance is the experimental evidence (3) that above certain 'critical velocities' the superfluid component loses its frictionless character and the liquid tends to behave as an ordinary fluid of density $\rho = \rho_n + \rho_s$ (where ρ is the 'total' density of liquid helium II, ρ_n is the density of the normal component, and ρ_s is the superfluid component density).

Assuming super-critical velocities, the drag on a sphere of radius 'a' and density ρ_a moving with terminal velocity 'V_T' through liquid helium II is, from equation (3)

$$D = \frac{C \pi a^2 \rho V_T^2}{2}$$

$$= \frac{4}{3} \pi a^3 \frac{(\rho_a - \rho) g}{} \qquad (5)$$

whence the drag coefficient is

$$C = \frac{8}{3} g \frac{(\rho_a - \rho)\, a}{\rho \quad V_T^2} \qquad (6)$$

where 'g' is the acceleration due to gravity.

The Reynolds number of the sphere is, from equation (4)

$$R = \frac{V_T d}{\nu} \qquad (7)$$

where d - sphere diameter

ν - kinematic viscosity of liquid helium II (based on the total density)

2.2 Significance of Measurements

Agreement of experimental C and R values as defined for helium II by equations (6) and (7) with the characteristic curve of Fig. A would support the Reynolds number as a suitable parameter of motion, and indicate boundary layer formation. Thus the 'ordinary fluid' concept for super-critical velocities would be strengthened.

Measurements at sub-critical velocities would be marked by deviations from the characteristic curve below a certain 'critical' Reynolds number. As only the normal component of density would then be contributing to the drag, C values based on equation (6) would drop and identification of a 'critical velocity' would be possible.

2.3 Previous Experiments

Three previous experiments on spheres moving through helium II have been reported:

Dowley, Firth, and Hallett (4) obtained data in the Reynolds number

range 10^2 to 10^3. Their values of the drag coefficient were significantly below the expected values even when they assumed that only the normal fluid was responsible for the drag and used the normal fluid density and viscosity in their calculations. These results indicate that the superfluid properties of helium II have not disappeared at these Reynolds numbers.

Laing and Rorschach (5) found drag coefficients of factors 2 to 5 higher than those for ordinary fluids in the region $R = .8 \times 10^5$ to 2×10^6. Also, they reported the absence of a drag crisis both in helium I and helium II, and attributed this to non-achievement of a steady-state boundary layer thickness.

O. Synko (6) investigated the Reynolds' number range 1.6×10^4 to 3×10^5. In the region $R = 3 \times 10^4$ to 3×10^5 he found good agreement with measurements made in other fluids. He also found no drag crisis and attributed its absence to the possibility that a true terminal velocity had not been reached. His work in the lower Reynolds' number range led him to conclude that the critical velocity is below his lowest velocity ... 10 cm. sec^{-1}.

2.4 The present work is an extension of the experiments of O. Synko. Its purpose is:

To re-examine the Reynolds number range about $R = 10^5$ for the drag crisis and to proceed to the higher Reynolds numbers attainable with the modified apparatus.

CHAPTER 3

APPARATUS

3.0 Remarks

Despite extensive modifications, the cryostat, as described in chapter 3 of reference (6) and outlined beside Fig. 3 of this work, remained unchanged in principle. Hence, the method of determining sphere velocities by timing between pulses produced at a photomultiplier tube by the sphere cutting light beams a known distance apart also remained unchanged. However, the cryostat and instrumentation suffered from a number of deficiencies which rendered the identification of terminal velocities difficult and, at times, impossible.

The slit and light guide systems were not completely free of relative movement. At times, sufficient movement would occur that perhaps one slit would be offset with respect to the light guide. Since verification of a terminal velocity required four input light beams to the phototube, measurements were then impossible because the electronics of the system was not sufficiently versatile to permit terminal velocity verification from three pulses. Even with four pulses available, the identification of a terminal velocity required two drops and the assumption of identical conditions for both. Clearly, an electronic system capable of verifying a terminal velocity from a minimum of 3 pulses for a single drop was desirable.

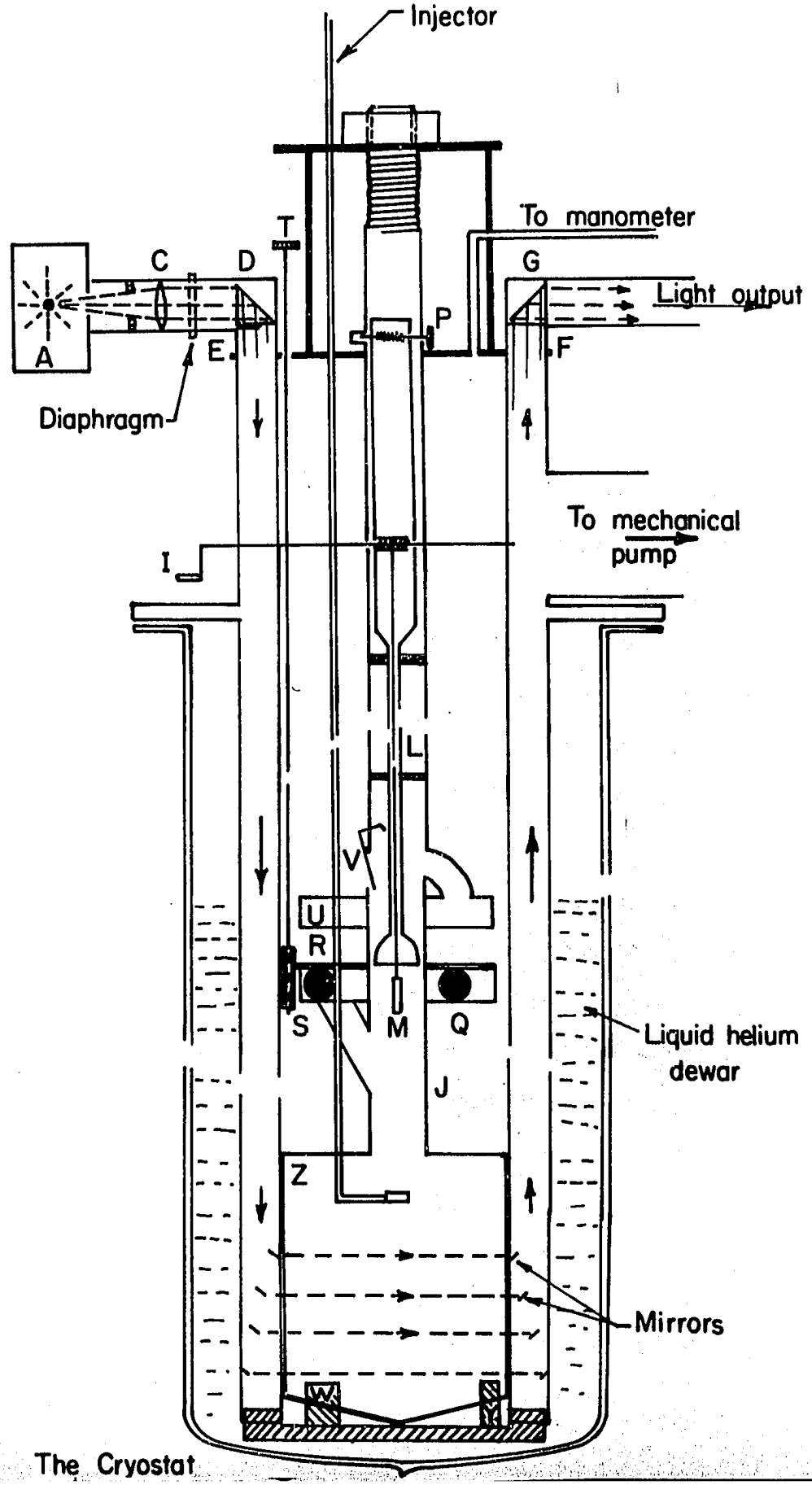

Fig. B The Cryostat

nometer

Light output

mechanical pump

Liquid helium dewar

Mirrors

THE CRYOSTAT

(Fig. B)

A) The Optical System

The Pointolite source A, the lens C, and the prism D, provided the means of supplying light to the slit and mirror systems mounted on the tubing E and F. These systems are described in section 3.1 of this work. The prism G reflected the light to the photomultiplier tube. The light path is indicated by arrows.

B) The Load and Storage Mechanisms

These mechanisms, some details of which may be seen in Fig. 4, were designed to permit measurements to be carried out on a number of spheres during a single 'run'. Initially, eight spheres were stored in the separate compartments of the 'magazine' chamber Q. This chamber, free to turn about the central column J, rested on a fixed plate which had a single hole in it leading to the chute S. By means of the rod T and the gear R, Q could be turned till a sphere fell through S into the lower chamber Z.

The magnet H lowered on a nylon string by means of the crank I could retrieve the sphere as many times as desired and raise it to the injector arm or to the end of the rod L for release. By use of the rack and pinion P, L could be raised from the top of Z to 14 cms. inside J.

When sufficient data had been obtained for a sphere, the trap V could be made to swing and block J by raising L, the sphere, and the magnet. The sphere could then be dropped upon V and through a chute into the storage chamber U. A new sphere could now be introduced from Q and the measuring process repeated.

C) The Temperature Control

The temperature of the helium was held constant to a few millidegrees by an A.C. Wheatstone bridge, one arm of which was the carbon resistor Y immersed in the helium. Slight variations in pumping speed were compensated for by reverse changes in the amplified off-balance bridge current to the heater element W.

The original cryostat provided no means of initially accelerating a sphere if it did not achieve terminal velocity under free fall conditions in the distance available.

The modifications to the system to overcome these deficiencies are outlined in the following sections.

3.1 Modifications of the Cryostat

The light guides on each side were replaced by four 15 by 3 mm. mirrors placed 3 cms. apart in stainless steal rectangular tubing. Each mirror was horizontally mounted on an axle, one end of which was supported by a bracket fastened to the tubing (Fig. 5). Thus opposite mirrors could be easily set parallel to each other and rotated to achieve four parallel beams of light across the lower chamber. Thin (.3 mm.) light beams were achieved by a slit system mounted on a plate soldered to the tubing (Fig. 5). The mounting of the slits on the plate prevented relative movement between the mirrors and the slits.

An iris diaphragm was incorporated beyond the lens at the light input to permit adjustment of the amount of light incident upon the mirrors (Fig. 2a). To permit variation of the light intensity, a rheostat was placed in the lamp circuit.

The solid bottom of the lower chamber (Fig. 5) was replaced by loose nylon netting to prevent damage to spheres upon impact. This system also ensured consistent centering of the sphere for easy magnet pick-up.

The maximum distance for free fall acceleration of spheres was increased to 29 cms. by extending the lower chamber by 9 cms.

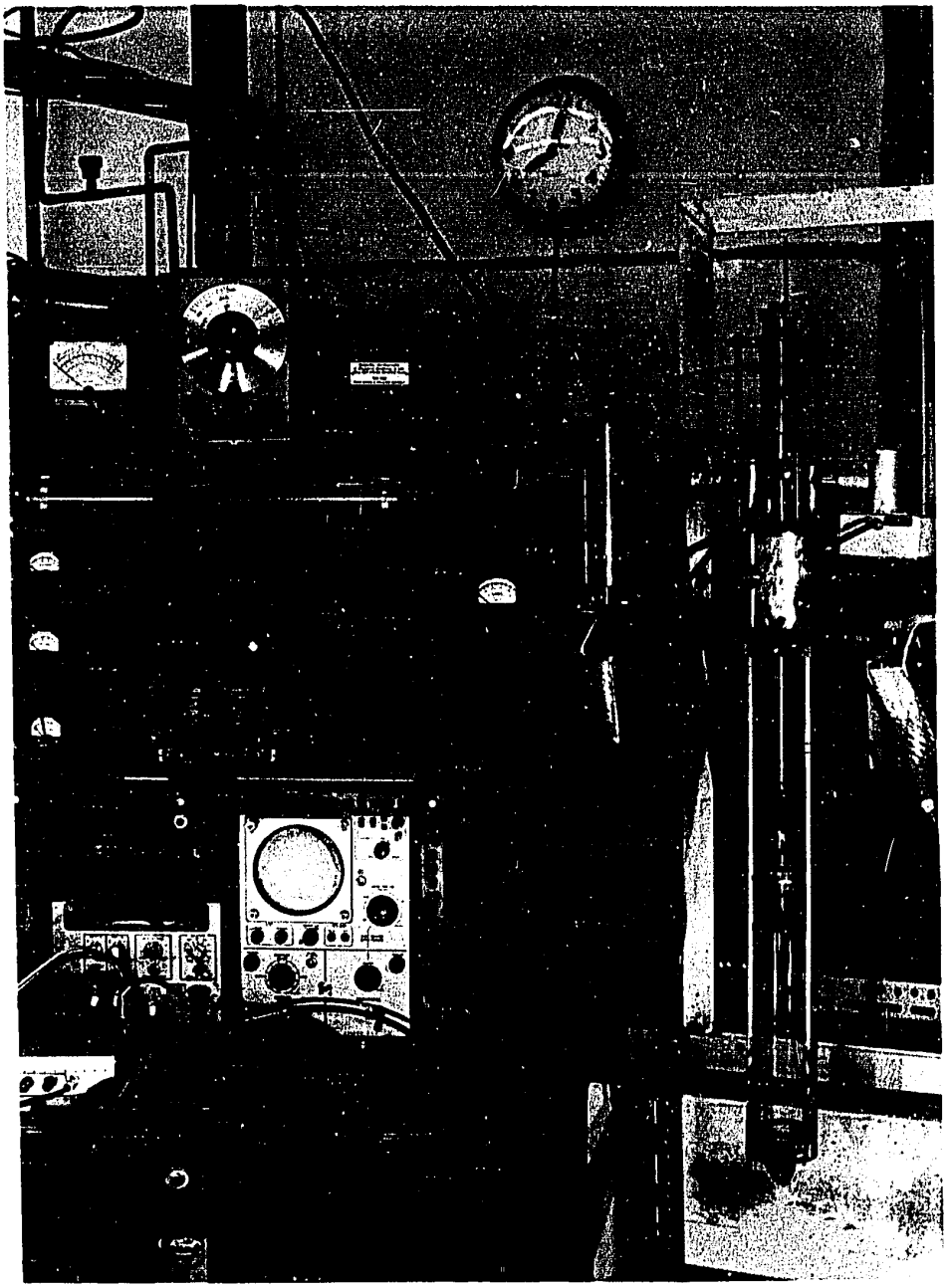

Figure 1. An overall view of the apparatus.

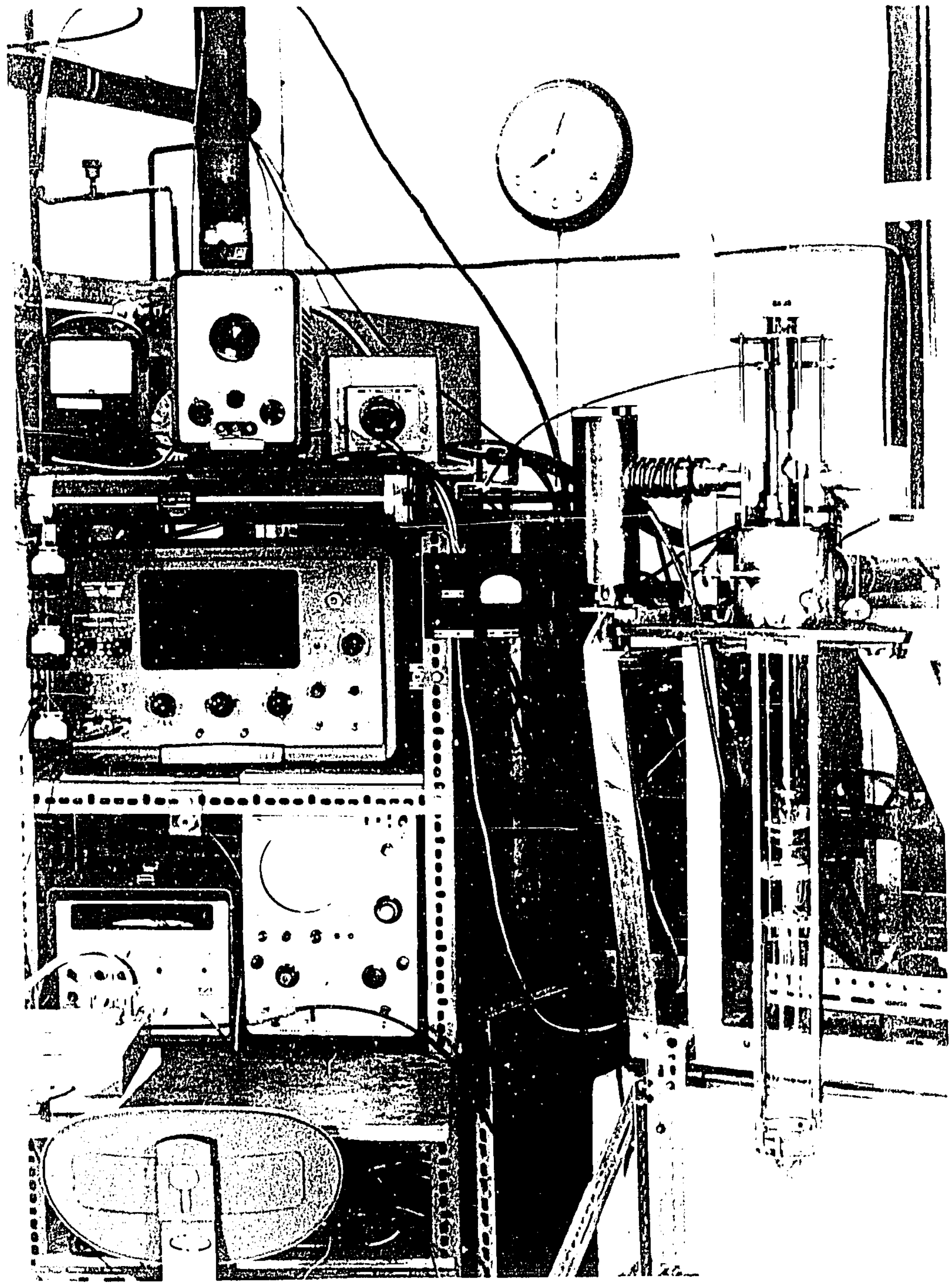

- a -

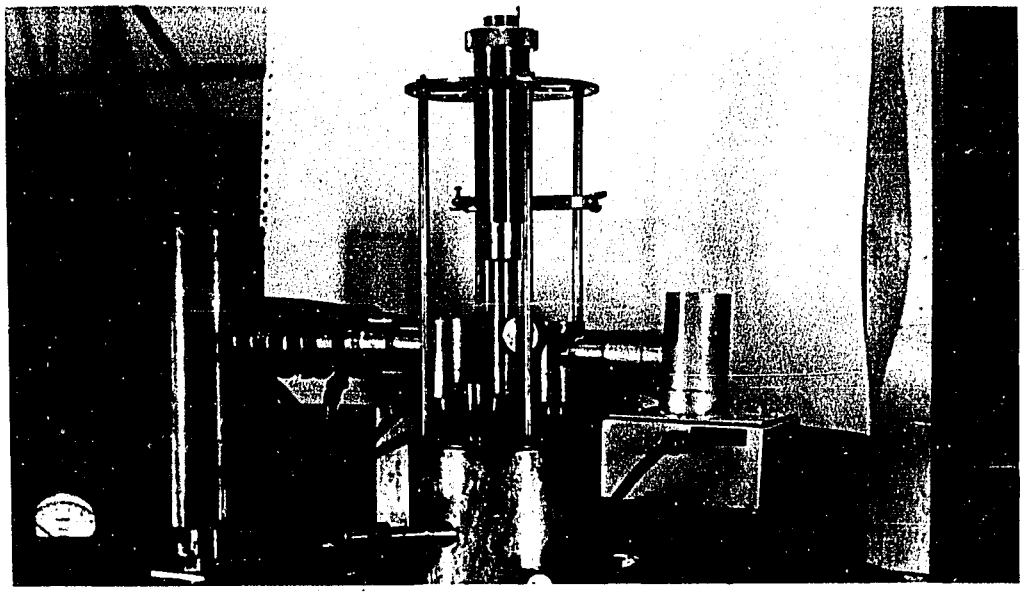

- b -

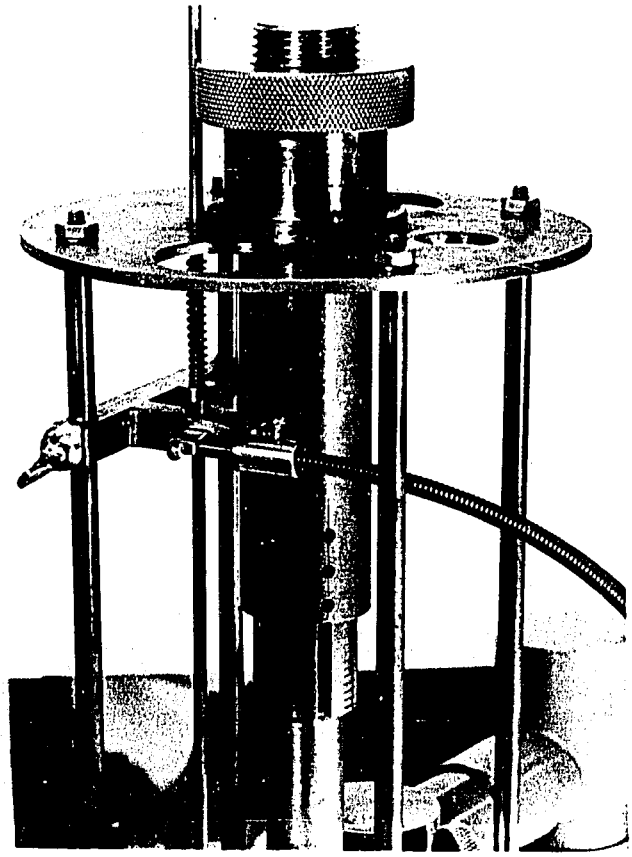

Figure 2. A view of the cryostat head.

- a -

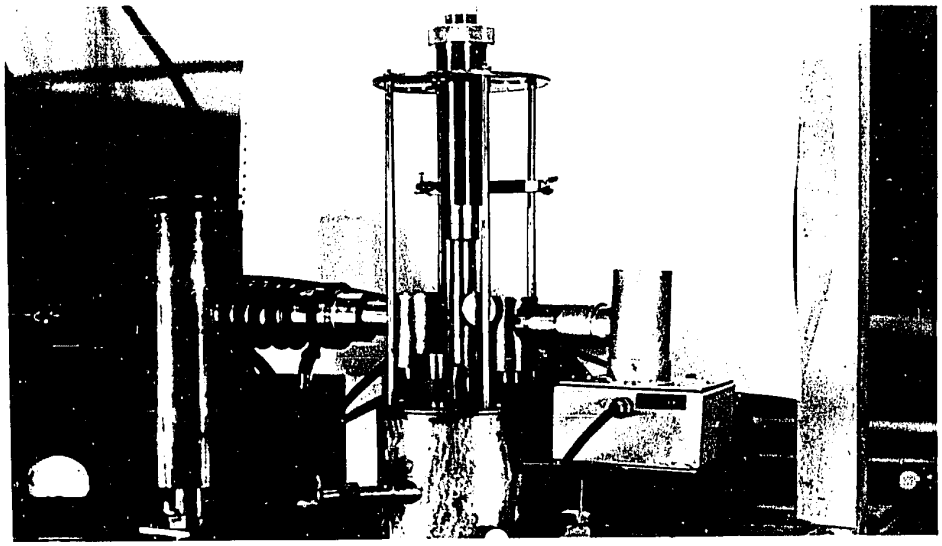

- b -

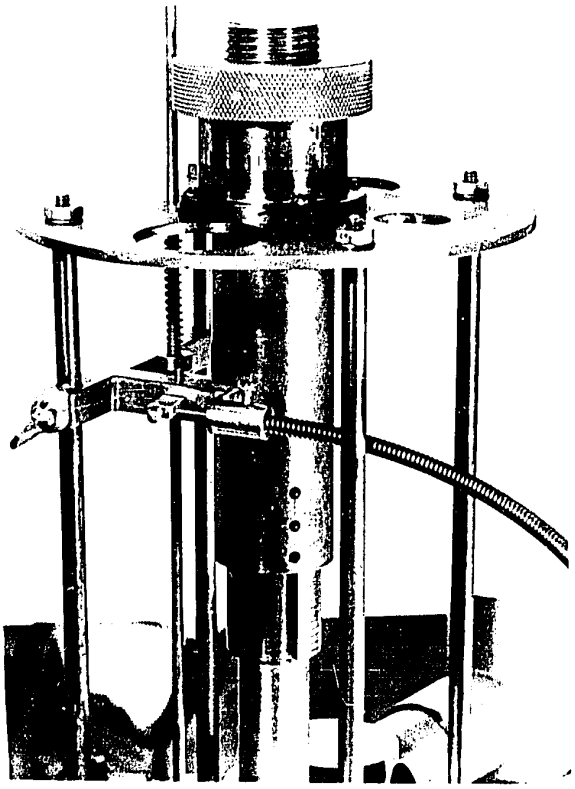

Figure 2. A view of the cryostat head.

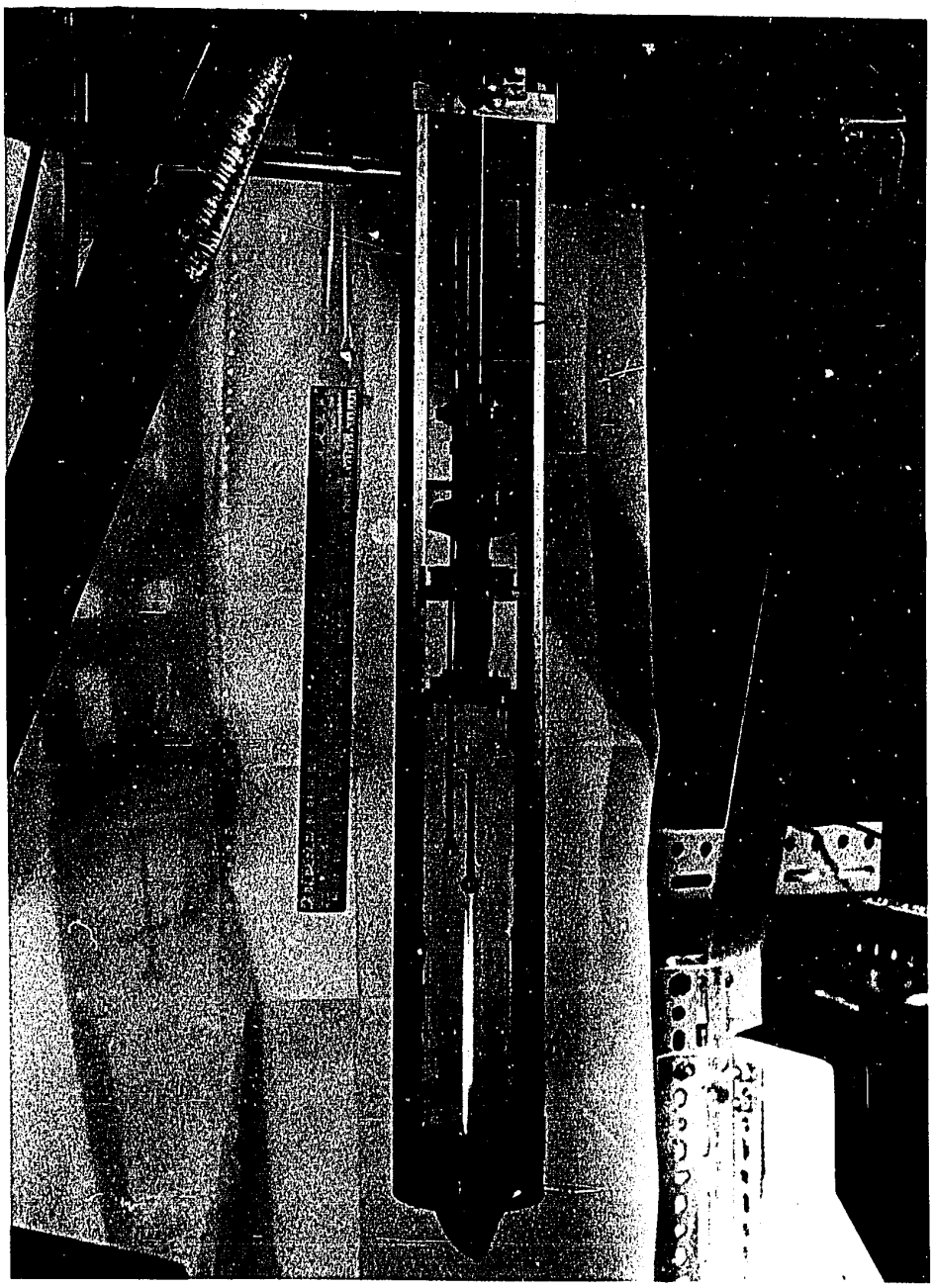

Figure 3. The lower unit of the cryostat.

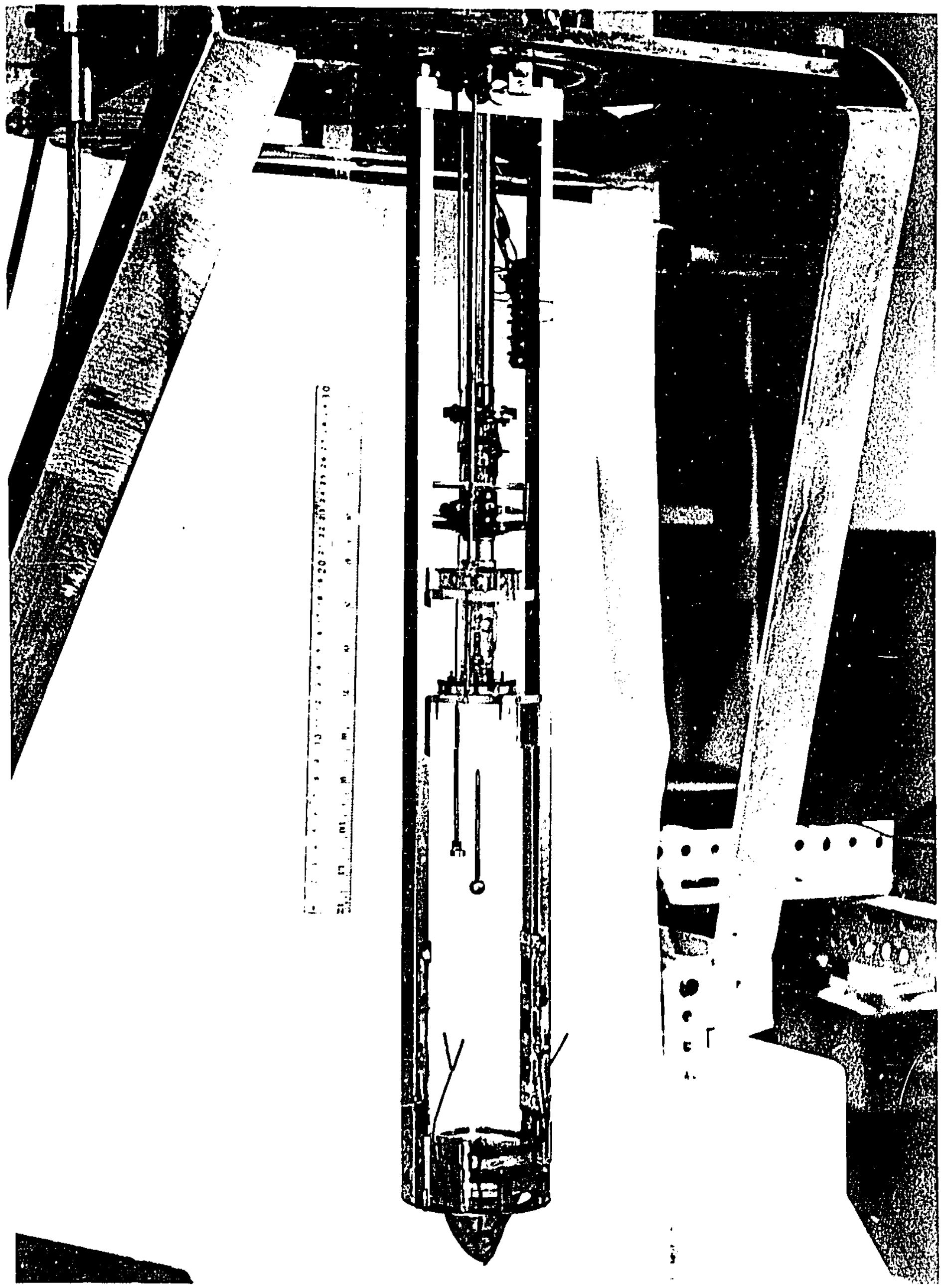

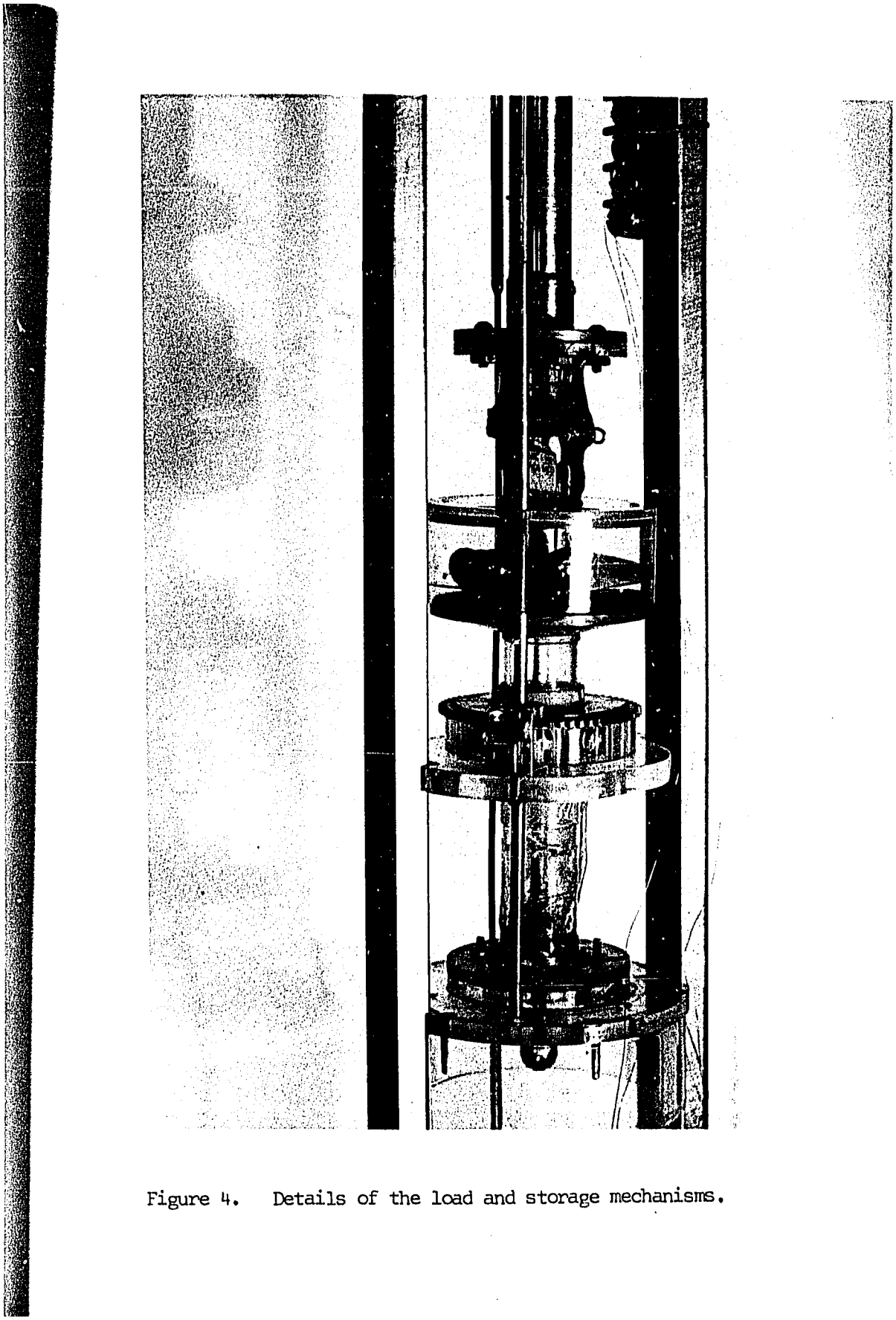

Figure 4. Details of the load and storage mechanisms.

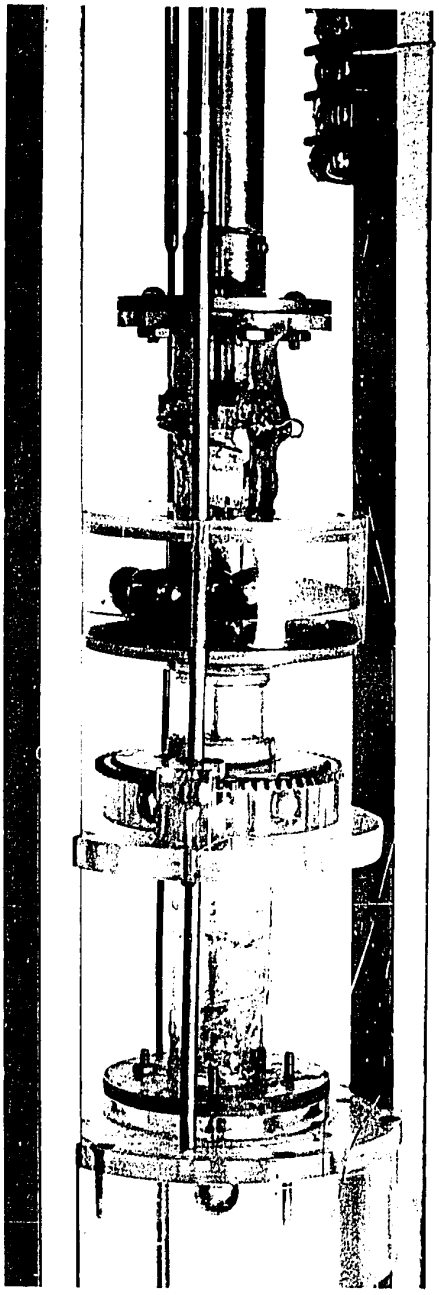

Figure 4. Details of the load and storage mechanisms.

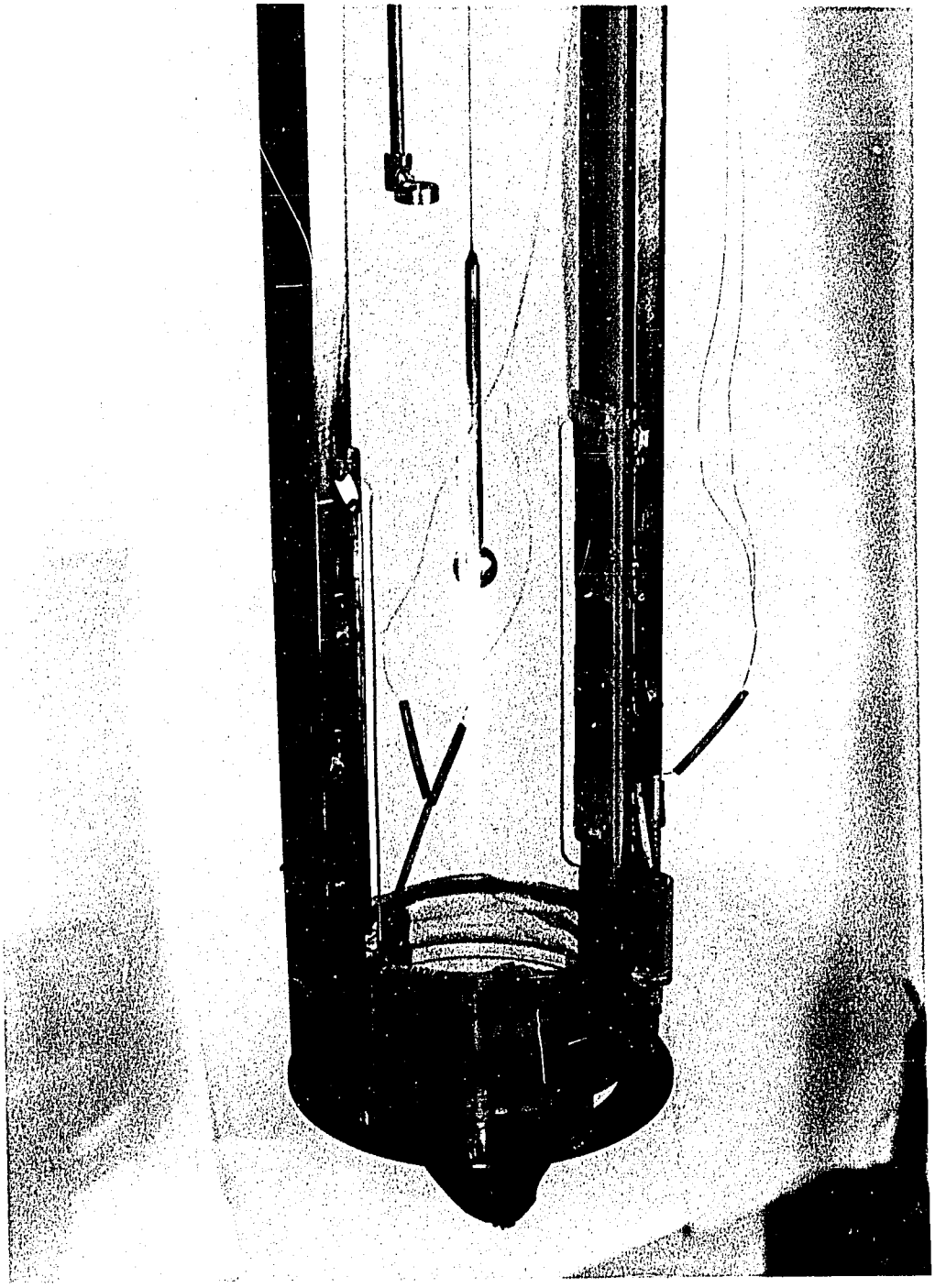

Figure 5. Details of the lower chamber.

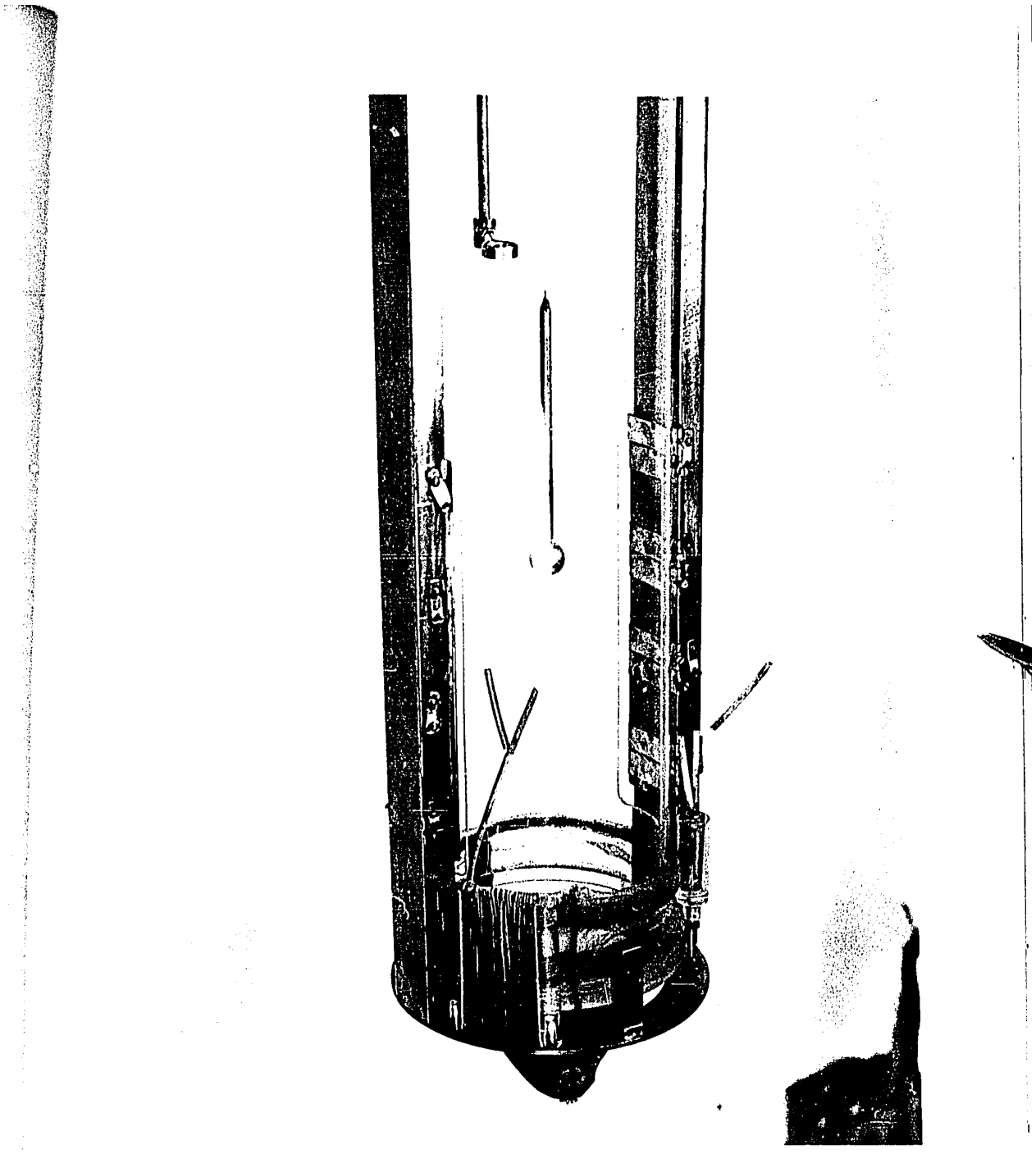

Figure 5. Details of the lower chamber.

To provide a means of initially accelerating those spheres unable to reach terminal velocity in the distance available, a spring-loaded injector (visible in Figures 3 and 5) was built into the cryostat. The rod passed off-center through the top of the lower chamber and through an O-ring seal at the cryostat head to a loading and trigger mechanism (Fig. 2b). This loading and trigger mechanism was designed to permit sphere injection from the same height within the chamber for variable degrees of compression of the spring. The exterior mounting of the spring permitted its replacement by one of different force constant or length at any time.

3.2 Electronic Circuitry

To permit terminal velocity verification from a single drop, the electronics of the system was completely redesigned. The circuitry assembled to permit timing between the pulses at the photomultiplier tube is shown in block diagram form in Fig. 6. The circuit diagrams of the components assembled by the author are shown (in Figures 7, 8, 9).

The emitter follower preamplifier (Fig. 7) preserved the pulse shape from the phototube. Its purpose was to drive the signal through the long cable necessary between the phototube and the other components of the system.

The Schmitt trigger (Fig. 8) produced a single standard output pulse for each input from the preamplifier. The standard pulse was required by the ring counter for reliable operation. The trigger was set to flip on pulses above the 'noise' level (20 mv.) caused by boil-off effects

at the tungsten bead light source.

To investigate the effect of this noise on the timing characteristics of the circuit, pulses of size, width and repetition times comparable to those encountered in actual measurements were introduced at the Schmitt trigger with a pulse generator. The times were studied on the counter for "clean" pulses from the pulse generator alone, and for pulses with the lamp noise superimposed. No significant variation was found.

The ring counter (Fig. 9) produced at separate outputs, one pulse for each input pulse. When reset, it stayed in the zero stage. A positive output pulse from the Schmitt trigger flipped it to the next stage. Unless the counter was reset after a fourth pulse, additional pulses were sent to ground through the transistor switch (S, Fig. 9) which turned on when the counter reached its fourth stage.

The two timing counters (Fig. 6) were set to "start" and "stop" on pulses sent to independent inputs from the separate outputs of the ring counter. Since the "stop" pulse at counter 1 could simultaneously be used as the "start" pulse at counter 2, times between any three consecutive pulses could be measured and a terminal velocity identified as readily as when two pairs of pulses were used. In addition, this system provided a means of timing between any chosen initial pulse and a following one. Hence, velocity measurements over 3, 6, or 9 cms. were possible. As the oscilloscope in the circuit (Fig. 6) provided a visual check on the pulses and their separation times, corresponding times and distances were easily identifiable.

at the tungsten bead light source.

To investigate the effect of this noise on the timing characteristics of the circuit, pulses of size, width and repetition times comparable to those encountered in actual measurements were introduced at the Schmitt trigger with a pulse generator. The times were studied on the counter for "clean" pulses from the pulse generator alone, and for pulses with the lamp noise superimposed. No significant variation was found.

The ring counter (Fig. 9) produced at separate outputs, one pulse for each input pulse. When reset, it stayed in the zero stage. A positive output pulse from the Schmitt trigger flipped it to the next stage. Unless the counter was reset after a fourth pulse, additional pulses were sent to ground through the transistor switch (S, Fig. 9) which turned on when the counter reached its fourth stage.

The two timing counters (Fig. 6) were set to "start" and "stop" on pulses sent to independent inputs from the separate outputs of the ring counter. Since the "stop" pulse at counter 1 could simultaneously be used as the "start" pulse at counter 2, times between any three consecutive pulses could be measured and a terminal velocity identified as readily as when two pairs of pulses were used. In addition, this system provided a means of timing between any chosen initial pulse and a following one. Hence, velocity measurements over 3, 6, or 9 cms. were possible. As the oscilloscope in the circuit (Fig. 6) provided a visual check on the pulses and their separation times, corresponding times and distances were easily identifiable.

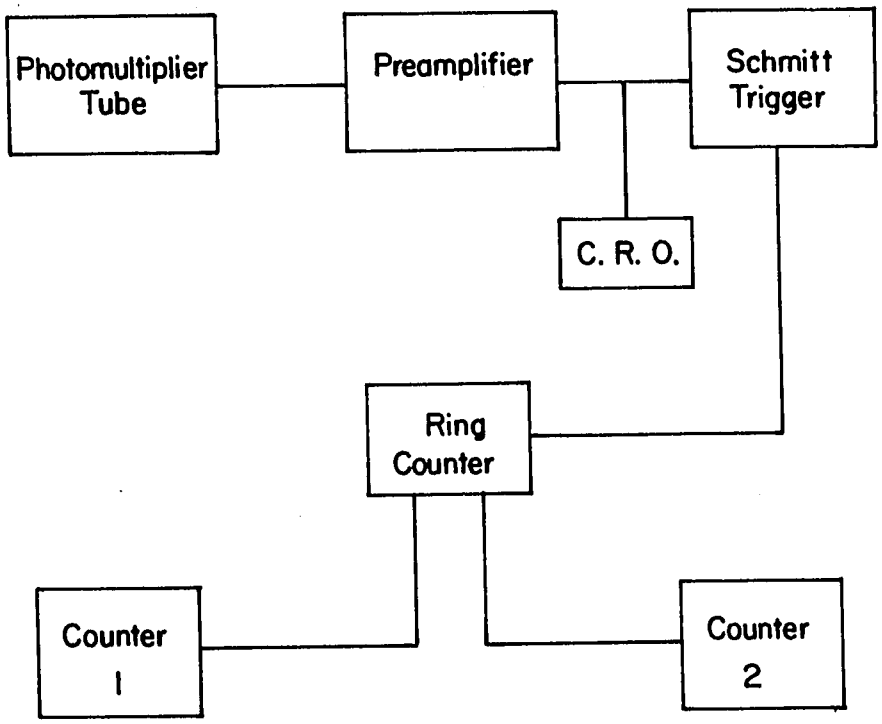

Fig. 6 Block Diagram of Electronic System.

4.2 Measurements of Terminal Velocity

Extensive measurements were carried out on spheres of density .2 to 1.2 gm. cm.$^{-3}$. The majority of runs was done in the temperature range 1.85 to 2.11 °K as determined by vapour pressure measurements with mercury and oil manometers and the "1958 He^4 Scale of Temperatures" (Ref. 9).

To minimize the effects of turbulence on the sphere path, a time of about 5 minutes was, in general, maintained between drops. However, the spheres often tended to deviate from a straight downward path. Since any path other than the straight and downward is of longer (and unknown) distance, any time then registered by a counter is of no real value as the velocity calculation is based on a distance of 3.00 cm.. It is possible for a sphere to follow a curved path which gives time measurements indicative of a terminal velocity. However, these times will yield terminal velocities smaller than the true ones; and the drag coefficients, which vary with V_T^2 will be markedly higher. As the ratio of 'straight' to 'curved' drops for any sphere was generally less than $\frac{1}{2}$, a simple averaging process of all the data accumulated while imposing the sole requirement that the counters show similar times, could seriously mask the true value of the terminal velocity. Consequently, a more rigid criterion for its identification had to be imposed.

When the narrow slits of the two dewars were aligned to give a view of the lower chamber, in the direction perpendicular to the plane between the 4 mirror pairs, the path of fall of a sphere could be well observed. A diagonal path of the sphere from one set of mirrors to the other

was readily evident, for the sphere quickly disappeared from view. Curved motion in the plane of the dewar slits was also indentifiable by direct viewing; However, the oscilloscope, which held a trace clearly for about 20 seconds, indicated this more readily by showing either the absence of some pulses, or 4 unequally spaced pulses.

When direct observation and the C.R.O. trace both indicated a straight downward path, the counters showed times which were clearly lower than those obtained under any other conditions. Hence, all the data accumulated for a sphere during a run was analyzed, and an average of the lowest times in not less than 10 drops was found. On the basis of this average minimum time, the two parameters C and R were calculated.

The difference in 'terminal times' indicated on counters 1 and 2 for a single drop was, on the average, 3%. The average variation in these times for a number of drops was about 2.5% from the mean. There is, therefore, an uncertainty of approximately 2.5% in the terminal velocities.

4.3 Sphere Contractions

Spheres of nickel, copper, and aluminum, were used in the measurements. The total contraction of the nickel spheres, manufactured by O. Symko (Ref. 6, P. 29), was measured by him to be .9%. From data in a paper by Fraser and Hallett (Ref. 10), the total contraction for the copper spheres was calculated as .3%. The total contraction of the aluminum

spheres was measured using a cathetometer and unsilvered dewars. This contraction was found to be about .2%, a value comparable to .4% calculated for aluminum through data of Ref. 10.

While these contractions give a relatively unimportant correction to the sphere diameter, they do become important in evaluating $(\rho_a - \rho)$ in equation 6. Hence, all the values of C were corrected for these sphere contractions.

4.4 Experimental Errors and Parameters

On the basis of the discussion in the preceding sections, the possible error in C through those in V_T^2 (5%), and d (1%), accumulates to about 6%. The uncertainty in R as a result of that in ν (10%), V_T, and d, is about 14%.

The variation of C vs. R obtained from the measurements carried out, has been plotted in Fig. 10 . Some of the results of O. Symko (Ref. 2, P. 35), as well as the appropriate portions of the universal curve have also been indicated. This figure is discussed in the following chapter.

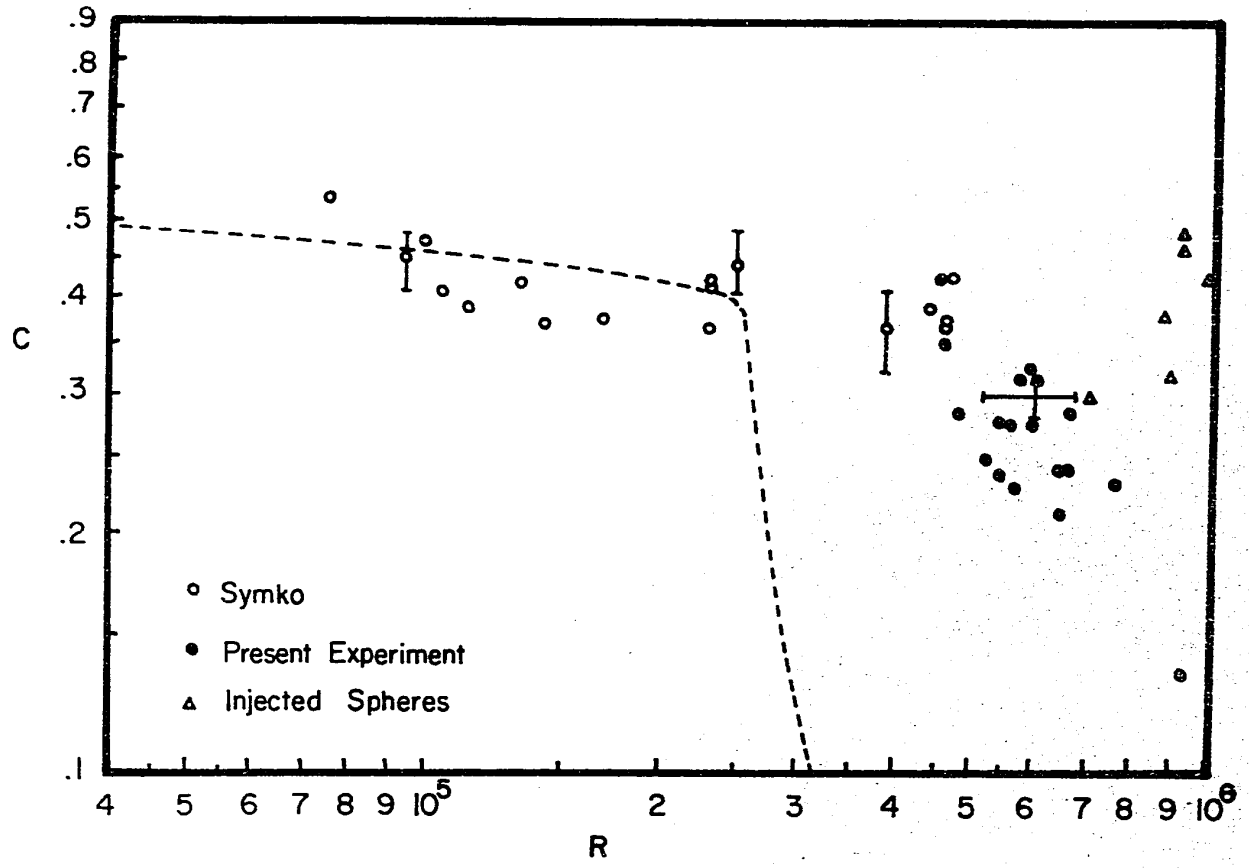

Fig. 10 Drag coefficient as a function of Reynolds number in liquid He II compared with the universal curve.

CHAPTER 5

DISCUSSION OF EXPERIMENTAL RESULTS

5.1 Analysis of Figure 10

The variation of the drag coefficient as a function of Reynolds number for spheres falling in He II is compared with the appropriate segment of the universal curve for spheres in Fig. 10. In addition to the author's points (Table 1), the figure also shows those of O. Symko which, upon analysis of his original data, conformed to the "minimum time" principle previously outlined.

In general, there is good agreement with the universal curve between $R = 7 \times 10^4$ and 2.6×10^5. For these Reynolds numbers, the spheres ranged in density from $\rho_a = .1$ to $.2$ gm. cm.$^{-3}$. A drop in the drag coefficient is clearly evident about $R \approx 4.5 \times 10^5$ ($\rho_a = .37$ gm. cm.$^{-3}$) where it begins to fall from about .45 to a minimum value of .13 at $R \approx 9.3 \times 10^5$ ($\rho_a = .48$ gm. cm.$^{-3}$). The drop is delayed, not as rapid as that indicated by the universal curve, but it is pronounced; and leads to the conclusion that there is a drag crisis in liquid helium II.

There are a number of possibilities as to why the drag crisis does not exactly duplicate that of the universal curve. Firstly: The onset of boundary layer turbulence, the cause of the drag crisis, is influenced by qualities of the sphere surface and other experimental factors. Accordingly, in given experiments, it may occur at higher or lower Reynolds numbers

even in ordinary fluids. Therefore, the delay noted above need not indicate a fundamental difference between liquid helium and other fluids at the high sphere velocities obtained. Secondly: As has previously been mentioned, a probable minimum uncertainty of 10% exists in the values of the kinematic viscosity (ν). It seems worthwhile to note that differences of the order of 30% occurred between some of the results from some of the experiments on which the average values calculated by Donnelly and Hallett (Ref. 7) are based. In addition, these experiments involved either motion of the liquid in bulk, or oscillatory measurements in which, after a first cycle, the measuring device moved through a disturbed fluid. In the present experiment, the sphere met "fresh" fluid throughout its path. There is, therefore, the possibility that the kinematic viscosity used may not precisely define the Reynolds numbers in He II for this experiment. However, providing that the variation in ν with temperature is not excessive, the definition of R in terms of it, still provides a consistent parameter through which the behaviour of the drag coefficients may be studied. This variation in the temperature range involved (1.85 to 2.11°K) is 12%. The uncertainty does not detract from the conclusion that there is a drag crisis in He II, for the drag coefficient is defined independently of ν. When the uncertainty in ν values is removed, it may well be that the drag crisis "position" in terms of R will coincide with that in ordinary fluids whose kinematic viscosities are more sharply defined.

Inasmuch as there is a drag crisis in He II, a boundary layer which becomes turbulent must form. Boundary layer formation is also strongly supported by the rising drag coefficients for spheres of density greater

than .48 gm. cm.$^{-3}$, which required acceleration to a terminal velocity by the injector. On the basis of the universal curve (Fig. A), a rise is to be expected, but not one of the magnitude or rate found. The correlation between these rising points and boundary layer formation is as follows:

Before a boundary layer can become turbulent, thus putting a sphere into the drag crisis region, it must first develop to a steady state thickness. For spheres of given diameter (d) and Reynolds number (R), this thickness (δ) may be approximated by the formula

$$\delta \approx 5\pi d\,(R)^{-1/2} \qquad \text{(Ref. 1, P. 24)}$$

The boundary layer thickness as a function of time, δ (t), on a suddenly accelerated wall is

$$\delta(t) \sim 4\,(\nu t)^{1/2} \qquad \text{(Ref. 1, P. 25)}$$

Assuming $\nu = 10^{-4}$ cm.^{2} sec.$^{-1}$, d = 1 cm., R = 10^6, these equations yield a time of 150 msec. necessary for the boundary layer to reach a steady state thickness. Assuming that the injector impulsively accelerates a sphere of R = 10^6 to a terminal velocity, the time that it takes to leave the injector, and reach the region in which its terminal velocity is measured, is only about 85 msec.. The time of the heaviest sphere not requiring injection, and dropped from within the central column is about 160 msec.. Therefore, the rise in drag coefficient for injected spheres appears to be due to the fact that the measured terminal velocity is smaller than that which would have been obtained if the boundary layer had had the time to reach a steady state thickness and become turbulent.

5.2 Conclusions

It has been shown that at the velocities attained by falling spheres in this experiment, the behaviour of liquid helium II tends to parallel that of ordinary fluids, in that the drag coefficient as a function of Reynolds number conforms, in general, to the characteristics of a universal curve. Uncertainties surrounding the values of the kinematic viscosity leave the precision of the Reynolds number in He II in doubt. However, the small variation in ν in the temperature range involved permits the use of R as a parameter through which the variation of the drag coefficient may be studied.

The presence of a marked decrease in the drag coefficient leads to the conclusion that there is a drag crisis in liquid helium II, and suggests the formation of a turbulent boundary layer. Boundary layer formation is further indicated by the supposition that the rising drag coefficient for injected spheres is due to the suppression of boundary layer turbulence.

On the basis of these considerations, the "ordinary fluid" concept of liquid helium II for super-critical velocities is strongly supported.

5.3 Further Experiments

As has been pointed out previously, the majority of measurements was carried out in a temperature range 1.85 to 2.11°K. At these temperatures, the ratio of superfluid density to total density is about .5. A series of measurements about 1.5°K, where this ratio approaches .9 would

5.2 Conclusions

It has been shown that at the velocities attained by falling spheres in this experiment, the behaviour of liquid helium II tends to parallel that of ordinary fluids, in that the drag coefficient as a function of Reynolds number conforms, in general, to the characteristics of a universal curve. Uncertainties surrounding the values of the kinematic viscosity leave the precision of the Reynolds number in He II in doubt. However, the small variation in ν in the temperature range involved permits the use of R as a parameter through which the variation of the drag coefficient may be studied.

The presence of a marked decrease in the drag coefficient leads to the conclusion that there is a drag crisis in liquid helium II, and suggests the formation of a turbulent boundary layer. Boundary layer formation is further indicated by the supposition that the rising drag coefficient for injected spheres is due to the suppression of boundary layer turbulence.

On the basis of these considerations, the "ordinary fluid" concept of liquid helium II for super-critical velocities is strongly supported.

5.3 Further Experiments

As has been pointed out previously, the majority of measurements was carried out in a temperature range 1.85 to 2.11°K. At these temperatures, the ratio of superfluid density to total density is about .5. A series of measurements about 1.5°K, where this ratio approaches .9 would

be of interest, and might aid in clarifying the role of the presently known values of the kinematic viscosity.

Assuming the suppression of boundary layer turbulence, it is clear that an attempt should be made to design a cryostat providing a longer path for injected spheres. Modification of the present system might be possible. Further analysis of the drag crisis region could then be carried out.

A detailed study of the effect of the walls on the experimental parameters should be made. Synko (Ref. 6, P. 38) examined the effect in a limited way, and suggested a correction of -5% to the experimental drag coefficients. This value is identical with that indicated by Laing and Rorschach (Ref. 5, P. 570).

APPENDIX

Table of Experimental Data

In the following table of experimental data, the sphere densities are those determined at room temperatures. The drag coefficients quoted have been corrected for sphere contractions.

Table I

Sphere Density ($gm.\ cm.^{-3}$)	Temperature (°K)	Velocity ($cm.\ sec^{-1}$)	Drag Coefficient (±6%)	Reynolds Number (±14%)$\times 10^5$
.341	2.12	80.7	.29	4.8
.332	2.09	84.1	.25	5.2
.373	2.05	70.7	.43	4.5
.373	2.08	73.3	.40	4.6
.349	2.07	89.6	.23	5.7
.332	2.06	85.8	.24	5.5
.492	2.11	98.1	.33	5.9
.904	2.10	146.5	.32	8.9
.484	2.06	149.7	.13	9.3
.440	2.07	91.3	.32	5.8
.492	2.07	104.8	.29	6.7
.332	1.94	79.4	.28	5.4
.349	1.93	81.6	.28	5.6
.363	1.84	85.8	.28	6.0
.373	1.87	93.3	.25	6.4
.379	2.06	100.1	.21	6.4
.441	2.10	106.3	.25	6.6
.452	1.82	110.8	.23	7.7
.513	1.96	104.6	.32	7.1
.840	2.00	129.6	.38	8.8
1.175	1.95	140.3	.47	9.3
1.208	2.00	140.4	.49	9.3
1.182	1.99	149.0	.43	10.0

REFERENCES

(1) Schlichting, H., Boundary Layer Theory, McGraw-Hill Book Co. Inc., N.Y. 1955, P. 16.

(2) Lane, C.T., Superfluid Physics, McGraw-Hill Book Co. Inc., 1962.

(3) Atkins, K.R., Liquid Helium, Cambridge, 1959, P. 199.

(4) Dowley, W.W., Firth, D.R., and Hallett, A.C.H., Low Temperature Physics and Chemistry, University of Wisconsin Press, Madison Wisconsin, 1958, P. 19. (Proceedings of the 5'th International Conference of Low Temperature Physics and Chemistry).

(5) Laing, R.A., and Rorschach, Jr., H.E., The Physics of Fluids, 1961, 4, 564.

(6) Symko, O., M.Sc. Thesis, University of Ottawa, 1962.

(7) Donnelly, R.J., and Hallett, A.C.H., Annals of Physics, 1958, 3, 320.

(8) Kerr, E.C., The Journal of Chemical Physics, 1957, 26, 511.

(9) U.S. Department of Commerce National Bureau of Standards, "The 1958 He^4 Scale of Temperatures" (NBS monograph 10).

(10) Fraser, D.B., and Hallett, A.C.H., Proceedings of the 7'th International Conference on Low Temperature Physics, P. 689.